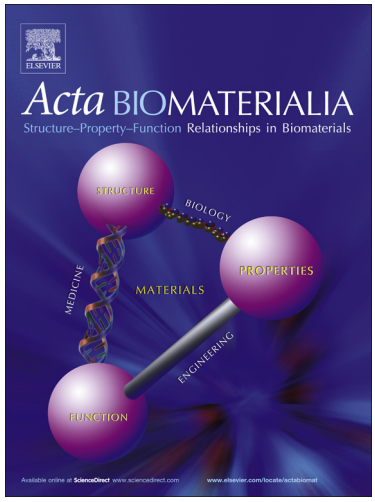

An optimized non-destructive protocol for testing mechanical properties in decellularized rabbit trachea

M Den Hondt, BM Vanaudenaerde, EF Maughan, CR Butler, C Crowley, EK Verbeken, SE Verleden, JJ Vranckx

PII: S1742-7061(17)30472-5
DOI: http://dx.doi.org/10.1016/j.actbio.2017.07.035
Reference: ACTBIO 5002

To appear in: *Acta Biomaterialia*

Received Date: 2 March 2017
Revised Date: 16 July 2017
Accepted Date: 20 July 2017

Please cite this article as: Den Hondt, M., Vanaudenaerde, B., Maughan, E., Butler, C., Crowley, C., Verbeken, E., Verleden, S., Vranckx, J., An optimized non-destructive protocol for testing mechanical properties in decellularized rabbit trachea, *Acta Biomaterialia* (2017), doi: http://dx.doi.org/10.1016/j.actbio.2017.07.035

An optimized non-destructive protocol for testing mechanical properties in decellularized rabbit trachea

Author list

Den Hondt M[a], Vanaudenaerde BM[b], Maughan EF[c], Butler CR[c], Crowley C[c], Verbeken EK[d], Verleden SE[b], Vranckx JJ[a]

Authors (surname, first name)

Den Hondt, Margot[a]	margot.denhondt@kuleuven.be
Vanaudenaerde, Bart M[b]	bart.vanaudenaerde@kuleuven.be
Maughan, Elizabeth F[c]	lizzie@maughans.net
Butler, Colin R[c]	colin.butler@ucl.ac.uk
Crowley, Claire[c]	claire.crowley.09@ucl.ac.uk
Verbeken, Eric K[d]	eric.verbeken@uzleuven.be
Verleden, Stijn E[b]	stijn.verleden@kuleuven.be
Vranckx, Jan J[a]	jan.vranckx@uzleuven.be

[a]Department of Plastic & Reconstructive Surgery, University Hospitals Leuven, Herestraat 49, 3000 Leuven, Belgium

[b]Lung Transplant Unit, Laboratory of Pulmonology, Department of Clinical and Experimental Medicine, KU Leuven — University of Leuven, Herestraat 49, 3000 Leuven, Belgium

[c]Department of Academic Surgery, Institute of Child Health, University College London, 30 Guilford Street, London, United Kingdom

[d]Department of Pathology, University Hospitals Leuven, Herestraat 49, 3000 Leuven, Belgium

Corresponding Author

Den Hondt Margot

Tel 0032 494 18 64 83

Fax 0032 16 34 87 23

margot.denhondt@kuleuven.be

Abstract

Successful tissue-engineered tracheal transplantation relies on the use of non-immunogenic constructs, which can vascularize rapidly, support epithelial growth, and retain mechanical properties to that of native

trachea. Current strategies to assess mechanical properties fail to evaluate the trachea to its physiological limits, and lead to irreversible destruction of the construct. Our aim was to develop and evaluate a novel non-destructive method for biomechanical testing of tracheae in a rabbit decellularization model. To validate the performance of this method, we simultaneously analyzed quantitative and qualitative graft changes in response to decellularization, as well as *in-vivo* biocompatibility of implanted scaffolds.

Rabbit tracheae underwent two, four and eight cycles of detergent-enzymatic decellularization. Biomechanical properties were analyzed by calculating luminal volume of progressively inflated and deflated tracheae with microCT. DNA, glycosaminoglycan and collagen contents were compared to native trachea. Scaffolds were prelaminated *in vivo*.

Native, two- and four-cycle tracheae showed equal mechanical properties. Collapsibility of eight-cycle tracheae was significantly increased from -40 cmH_2O (-3.9 kPa). Implantation of two- and four-cycle decellularized scaffolds resulted in favorable flap-ingrowth; eight-cycle tracheae showed inadequate integration.

We showed a more limited detergent-enzymatic decellularization successfully removing non-cartilaginous immunogenic matter without compromising extracellular matrix content or mechanical stability. With progressive cycles of decellularization, important loss of functional integrity was detected upon mechanical testing and *in-vivo* implantation. This instability was not revealed by conventional quantitative nor qualitative architectural analyses. These experiments suggest that non-destructive, functional evaluation, e.g. by microCT, may serve as an important tool for mechanical screening of scaffolds before clinical implementation.

Introduction

Tracheal tissue-engineering technology stands to benefit a variety of patients suffering end-stage benign and malignant tracheal pathologies that comprise more than half the length of the organ. Definitive replacement aims to radically extend and improve quality of life. Such transplantation demands the creation of a non-immunogenic construct that supports rapid revascularization and regenerates a ciliated epithelium. The trachea, as a hollow tube, has often been thought to be a straightforward structure to recreate *de novo*. However, this simplicity has been deceptive [1,2,3]. It has become clear from both pre-clinical and clinical cases that further optimization of scaffold-material is required [4]. Decellularization is a front-running strategy to generate scaffolds since it selectively removes cellular material within the trachea, leaving a non-immunogenic framework of extracellular matrix.

Preservation of tracheal biomechanical properties is paramount for successful clinical transplantation. Collapsing or stenosing grafts require endoluminal stenting [1,2], which is associated with significant morbidity and does not offer a long-term solution. Furthermore stent-associated complications are a valid criterion for patients to be considered for tracheal transplantation [5]. Clinical experience to date with both tracheal allografts and tissue-engineered tracheae has suggested that collapse of a tracheal graft post-implantation might occur for multiple reasons such as insufficient vascularization, infection, failed repopulation and chondrogenesis, and remodeling after implantation [1,2,6,7]. Moreover, the extracellular matrix (ECM) framework of the grafts may not be mechanically robust compared to native tissue as a result of the *in-vitro* decellularization process [8].

Biomechanical characteristics of the tracheal cartilaginous framework and various bio-engineered tracheal grafts [9,10,11] have been extensively examined, however studies have generally assumed the trachea to be a radially-symmetrical object [12] despite tracheal anatomy being clearly non-symmetrical in nature [13,14]. Testing has therefore focused on uniaxial tensile properties, which established significant differences in mechanical behavior of the trachea only at high cycle-numbers of detergent-enzymatic decellularization [9,10,11,15]. These assay methods offer us little insight into the more physiologically-relevant preservation of graft strength under varying intraluminal pressures. In 2012, Haykal *et al* led the way in this thought process by proposing a new model for testing compliance and collapsibility of decellularized trachea by mimicking natural movements of breathing [16].

The aim of this study was to further develop a novel, non-destructive method for tracheal biomechanical testing that can be used as a tool for mechanical screening of scaffolds prior to clinical implementation. To reach this goal, we assessed the extent to which functional mechanical properties of rabbit tracheae were affected with increasing degrees of detergent-enzymatic decellularization using physiologically-relevant parameters of compliance and collapsibility [17,18,19,20]. Endoluminal volumes of progressively inflated and deflated tracheae were calculated with micro-computed tomography (microCT). To validate the performance of this microCT-technique, we simultaneously analyzed quantitative and qualitative architectural changes within grafts in response to decellularization, as well as *in-vivo* biocompatibility of implanted decellularized scaffolds.

Materials and Methods

2.1 Tracheal procurement and decellularization

Rabbits were treated according to the European Directive on the Protection of Animals. The Ethical Committee for Animal Experimentation of the University of Leuven approved the study protocol (P115/2012).

New Zealand White Rabbits weighing 2.9 ± 0.3 kg underwent terminal anesthesia using ketamine 40 mg/kg and xylazine 6 mg/kg intramuscularly and a lethal dose of T_{61} 0.3 ml/kg intravenously. Tracheae were circularly detached from surrounding tissues over their entire length, carefully cleaned of residual blood and adventitial tissue and rinsed with phosphate-buffered saline (PBS). Samples were immediately transported on ice.

Tracheae underwent 0 (control) to 8 cycles of detergent-enzymatic decellularization, following a clinically-used protocol established by Conconi *et al* and Meezan *et al* [17,18]. Briefly, samples for decellularization were washed in sterile distilled water (dH_2O) with 1% penicillin-streptomycin and amphotericin B at 4°C for 72 hours. Each 48-hour cycle commenced with a 4-hour detergent treatment with sodium deoxycholate (SDC) 4% (Sigma) at room temperature to rupture cellular membranes, followed by a 3-hour incubation step at 37°C with 1mM sodium chloride solution containing 50 kU/ml DNAse (Thermo Fisher) to digest exposed DNA. Tracheae were washed with PBS to remove remaining reagents between steps. Samples were then mechanically agitated at 4°C in sterile dH_2O with antibiotics and antimycotic for 41 hours. Following the last cycle, washing with dH_2O was extended to 72 hours. Lastly, tracheae were mechanically agitated in PBS at 4°C for 48 hours.

2.2 MicroCT-scanning and volume calculation

Haykal *et al* defined the clinical range of tracheal pressure-differences between -81.6 cmH_2O (-8.0 kPa) and +13.6 cmH_2O (+1.3 kPa) [16]. We repeated the determination of a relevant pressure-range for scanning, by testing the pressure system on eight healthy human subjects (age 26 - 62). During normal breathing, mean pressure-changes varied between ±6.7 ± 2.9 cmH_2O (mean ± standard deviation). During forced inspiration and expiration, mean pressure-changes recorded were -87.3 ± 9.3 cmH_2O and +72.0 ± 10.8 cmH_2O respectively. We therefore decided to scan rabbit tracheae between -100 cmH_2O (-9.8 kPa) and +80 cmH_2O (+7.8 kPa).

24 tracheae, which underwent 0 (control), 2, 4 and 8 cycles of detergent-enzymatic decellularization, were used for scanning (n = 6 per group). Tracheae, each 6 cm in length, were suspended by the ends within the sample holder of the microCT scanner (Skyscan 1076 Bruker microCT, Kontich, Belgium) (**Fig. 1**). One end of the construct was sealed onto a closed 1-way stopcock, whilst the other end was connected to a tubing system with a 3-way stopcock. This 3-way stopcock was also connected to a liquid-column manometer filled with water and a 50 cc syringe with a syringe-driver to gradually increase and decrease luminal pressure. The pressure throughout the whole system was continuous and thus identical. The liquid-column manometer allowed us to control and quickly correct minimal pressure-changes during scanning, caused by small air leaks. The tracheal connection was filled with air, mimicking normal physiology. After obtaining each pressure point, the trachea was scanned statically over a central length of 2.5 cm. Specimens were scanned at 50 kV, 178 µA and maximal power (10 W). 360° rotation with 0.7° rotation steps were used. The filter was set at 0.5 mm aluminium, the exposure time was 316 ms. Datasets were reconstructed with NRecon (Bruker microCT) and converted to DICOM-files for volumetric analysis and three-dimensional reconstruction (Osirix, Osirix Foundation).

2.3 Spectrophotometric Quantification of DNA, Glycosaminoglycans (GAGs) and Collagen

All spectrophotometric recording was performed using a Tecan Infinity microplate reader [21]. Total DNA-, sulfated-glycosaminoglycan (sGAG) and collagen-content persisting within native and decellularized trachea (1 to 8 cycles) were assessed. To determine total DNA, samples were homogenized in lysis buffer (50 mM Tris-HCl, 50 mM EDTA, 1% SDS and 10 mM NaCl), before overnight digestion with proteinase K. DNA was extracted in phenol/chloroform, precipitated with 100% ethanol, washed with 70% ethanol and redissolved in ribonuclease-free water. DNA was then characterized for purity and yield at optical densities of 260 nm and 280 nm absorbance and quantified at an optical density of 280 nm absorbance.

Total sulfated-glycosaminoglycan (sGAG) content was quantified using the Blyscan GAG Assay Kit (Biocolor, UK). Briefly, 50 mg (wet weight) of homogenized tissue was incubated with Papain digestion-buffer at 65°C for 18 hours, with occasional vortexing. Samples were incubated with 1,9-dimethyl-methylene blue dye and reagents according to the manufacturer's instructions.

Spectrophotometric analysis was performed at 595 nm. Obtained data were read against a standard curve of known chondroitin-4-sulfate concentrations to calculate total sGAG-content.

Total collagen-content was quantified using the SIRCOL collagen assay (Biocolor, UK). Collagen was extracted from homogenized samples into 0.5 M acetic acid and incubated with Sirius red dye before analysis at an optical density of 555 nm absorbance. Readings were compared to a standard curve of known collagen-concentrations to calculate tissue-collagen content.

2.4 *In-vivo* implantation of decellularized scaffolds

Two- (n = 6), four- (n = 6) and eight-cycle decellularized rabbit tracheae of 3 cm length (n = 6) were implanted heterotopically, within the recipient's lateral thoracic artery flap, as described previously [22]. Enrofloxacin per os was given up until termination of the experiment. Constructs were monitored for 21 days.

2.5 Histology and immunohistochemistry

Samples were fixed in 10% neutral buffered formalin and embedded in paraffin. Sections were stained with hematoxylin and eosin (H&E), Masson's Trichrome (MT), periodic acid shiff (PAS), picrosirius red (PR) and Safranin O according to standard protocols. H&E was used to detect remaining nuclei after decellularization and to evaluate flap ingrowth after *in-vivo* implantation, PAS-staining was applied to evaluate basement membranes, Safranin O dye with Fast Green counterstain revealed proteoglycans and collagen respectively. MT- and PR-stained samples were also used for collagen visualization. The latter stain was used under polarizing light to assess collagen-fiber organization. To identify the presence of any remaining nuclear material, samples were pretreated with antigen retrieval buffer Tris/EDTA (pH 9) in the Dako PT module before incubation with 4',6-diamidino-2-phenylindole (DAPI 1:2000, Thermo Fisher) for 15 minutes.

Implanted tracheae were also stained with CD31 to assess revascularization and CD4 and CD8 to assess *in-vivo* biocompatibility. Endothelium was visualized with CD31-incubation (dilution 1:50, CD31/PECAM1 mouse anti-rabbit monoclonal antibody, Novus Biologicals) for 30 minutes after pretreatment with Tris/EDTA (pH 9). Secondary mouse-envision HRP-labeled antibodies (DAKO) were applied for 30 minutes. Staining was completed by a ten-minute incubation with 3,3'-diaminobenzidine

(DAB)+ substrate-chromogen, resulting in a brown-colored precipitate at the antigen site. To determine lymphocytic infiltration, frozen tissue samples were incubated with primary antibody CD4 (dilution 1:50, CD4 mouse anti-rabbit monoclonal antibody, LifeSpan BioSciences) or CD8 (dilution 1:50, CD8-alpha mouse anti-rabbit monoclonal antibody, Novus Biologicals) for 30 minutes. Following treatment steps were applied as described above.

Stained tissue sections were mounted, coated and visualized via conventional light, polarized light and fluorescence microscopy (Olympus BX61).

2.6 Scanning electron microscopy (SEM)

SEM-images of the cross-section, top and bottom surfaces of the decellularized scaffold were taken to examine surface-topography of the material. Samples were fixed in 2.5% glutaraldehyde (Sigma; G5882). Scaffolds were first washed in 0.1m phosphate buffer (pH 7.4) followed by dH_2O. Specimens were then dehydrated in a graded ethanol-water series to 100% ethanol and critical point-dried using CO_2. Next, samples were mounted onto aluminium stubs using sticky carbon taps, so that the surfaces of interest were presented to the beam. Samples were coated with a 2 nm-thin layer of Au/Pd using a Gatan ion-beam coater, and viewed using a Jeol 7401 FEG-SEM.

2.7 Statistical analysis

Statistical analyses were carried out using GraphPad Prism 6 software. Two-way ANOVA analysis with Bonferroni post-testing was used for microCT-measurements to compare each group to all other groups (significance threshold of $p < 0.05$). One-way ANOVA analysis with post-hoc Bonferroni was used for DNA-, sGAG- and collagen-quantification.

Results

3.1 MicroCT scanning and volume calculation

MicroCT was used to determine physiological biomechanical properties of progressively inflated and deflated tracheae. Compared to native tracheae, we found an increased collapsibility of 8-cycle tracheae (**Fig. 2**). Significant differences were seen at luminal pressure-changes below -40 cmH_2O (**Table 1**). At -100 cmH_2O, 8-cycle tracheae also showed significantly more structural weakening than 2-cycle tracheae. The other groups showed no significant differences. In the positive pressure-range, we found no increased compliance between any of the groups (**Fig. 3**). Tracheae deformed preferentially at the trachealis muscle and the transition between cartilage rings and trachealis muscle (**Fig. 2**). More extreme negative pressure-changes elicited curving of 8-cycle tracheae at various locations along the tracheal circumference. We observed no location-specific pattern of collapse at the proximal versus distal part of scanned tracheae.

3.2 Quantification of DNA, Glycosaminoglycans and Collagen

We observed a steady reduction in mean total DNA-content with successive decellularization cycles. This drop was non-significant between each successive cycle in isolation, but cumulatively significant up to cycle 4 (**Fig. 4 a**). Additional decellularization after this point did not show any further significant difference in DNA-content, with a mean of 105 ng/mg at 8 cycles. No significant reduction in total sGAG was seen in the decellularization process. Collagen-content showed a steady relative increase. This increase was significant between native trachea and cycle 8, and between cycle 2 and cycle 8 (**Fig. 4 b, c**).

3.3 Histology

From decellularization cycle 2 onwards, cellular elements were negligible in non-cartilaginous tissue on H&E and Masson's Trichrome staining (**Fig. 5**). This was confirmed on DAPI-stains. Chondrocyte-nuclei remained present up until 4 cycles, with normal eu- and heterochromatin content. After 8 cycles of decellularization, chondrocytes were scarce, with increasing loss of normal morphology. On DAPI-staining, we did not find residual DNA-fragments attached to ECM-fibers of decellularized scaffolds. However, we witnessed considerable residual DNA-staining within the cartilage. These fragments were highly condensed within nuclei of native tracheae. With increasing cycle-numbers, the intensity of the fluorescent signal diminished, and coloration became more dispersed.

The overall structure of the ECM was preserved within each group. Qualitative analysis of sGAGs on Safranin O stain with Fast Green counterstain revealed normal presence of these mucopolysaccharides up to eight cycles. Picrosirius-red sections under polarizing light showed normal collagen-organization within the outer layers of the cartilage. However, the upper submucosal layers showed less structured, divergent collagen-fibrils after eight cycles of decellularization. Von Kossa staining demonstrated that extracellular cartilaginous calcifications were present in all groups.

3.4 Electron microscopy

Native tracheae had a normal ciliated epithelial covering (**Fig. 6**). Mucosal cells were effectively removed from all decellularized constructs. The basement membrane showed an intact *lamina basalis* for 2- and 4-cycle tracheae compared to 8-cycle decellularized tracheae, which had large gaps exposing the underlying reticular collagen-fibrils. The 3D-architecture of the cartilaginous scaffold was otherwise preserved up to 8 cycles (**Fig. 7**).

3.5 *In-vivo* implantation of decellularized scaffolds

Whereas eight-cycle tracheae consistently showed inadequate integration within the flap, two- and four-cycle constructs successfully adhered onto the flap externally (**Fig. 8**). Eight-cycle grafts were covered with a florid mixed neutrophilic-eosinophilic inflammatory infiltrate internally as well as externally, impeding flap-ingrowth. None of the constructs however, showed satisfactory revascularization of the submucosal space. No immunological response directed towards the cartilage was detected. We witnessed only scarce CD4+ and CD8+ lymphocytes, located within the adventitia.

Discussion

The main function of the trachea is to maintain an open conduit for air passage, withstanding a wide range of intrathoracic pressures. Biomechanical properties of this semi-rigid, semi-flexible tube are fundamental to successful trachea transplantation. In this study, we refined an innovative technique for testing these properties. The technique demonstrated that incompletely decellularized rabbit tracheae may already have an increased collapsibility within a physiological pressure-range. In our series, tracheae collapsed more readily after eight cycles of decellularization.

Whilst these findings in rabbits can be interpreted as relative values, it is not always possible to extrapolate the number of decellularization-cycles needed to obtain complete cell-removal between species. Also the threshold for loss of mechanical properties differs among species, as demonstrated by the following data. Zang *et al* were able to remove all major histocompatibility complex (MHC) antigens in non-cartilaginous sections of rat trachea after only 1 cycle [9] with complete removal of chondrocytes after 5 cycles. Despite the absence of a significant difference in strain at failure by uniaxial tensile testing, manual compression of the construct suggested weakening after 5 cycles of decellularization. Sun *et al* found absence of (sub)mucosal cells of rabbit trachea following the initial dH_2O-incubation stage. Uniaxial testing was not significantly altered in rabbit trachea up to 7 cycles of detergent-enzymatic decellularization [15]. Evidently, the more complex the species, the more cycles are needed to remove all cells and to influence mechanical integrity. Conconi *et al* reported a persistence of chondrocytes even after 18 cycles of decellularization of porcine trachea [17]; complete removal of cells required 22 cycles, albeit at the expense of loss of structural integrity. Partington *et al* also found a decrease in porcine tracheal GAG-content and DNA accumulation along ECM-fibers from 20 cycles on, with incomplete removal of chondrocytes even after 25 cycles [8]. Uniaxial tensile testing showed no significant difference in tensile moduli up to 20 cycles. Though, from 25 cycles on, they reported reduced stiffness compared to native trachea. Similarly, Jungebluth *et al* reported few residual chondrocytes after 17 cycles of decellularization in pig trachea and preserved mechanical properties on uniaxial tensile testing [10]. However, they observed loss of strain ability after 20 cycles. Haykal *et al* found equal cell removal after 17 cycles of detergent-enzymatic decellularization in pig trachea [16]. Furthermore, they demonstrated continued positive MHC-staining in the submucosal glands at even higher cycle-numbers. Using the clinically-established protocol of Conconi and De Coppi [17,18,19,20], it is known that adult human trachea requires higher cycle-numbers akin to pigs to achieve cell clearance. Baiguera *et al* reported nearly complete removal of cells and preservation of

uniaxial tensile properties after 25 cycles of human tracheal decellularization [11]. Presumably, also differences in tracheal tissue-architecture and composition explain these differences. E.g. it is known that rabbit trachea contains more submucosal vascular structures compared to the more glandular submucosa of human trachea [22,23].

Traditional mechanical studies employ uniaxial tensile testing to assert that tracheal mechanical strength is relatively preserved, even following high numbers of decellularization cycles. By these methods, elastic moduli vary within a range of around 1 MPa to 63 MPa [8,9,12], depending on the tested species. For ultimate tensile strength, values up to 14 MPa have been reported [8,9,12]. However, if we convert this SI pressure unit to cmH_2O, these studies measure uniaxial tracheal characteristics within the range of 1×10^4 to 6.3×10^5 cmH_2O. Yet, grafts must cope with up to 10^5 smaller physiological pressure-changes during normal respiration. Moreover, as Teng *et al* described in their mathematical model, the assumption that the cartilage is a symmetrical ring causes large errors in predicted airway compliance and trachealis muscle stress [14], and therefore, should not be used in tracheal mechanical simulation. Taking this non-linear behavior of the trachea into account, we optimized a novel microCT method for biomechanical testing of trachea developed by Haykal *et al* [16]. They scanned 15 porcine tracheae to compare native controls to those prepared by three different decellularization protocols using 1, 9 and 17 treatment-cycles. They indicated that tracheae collapsed more readily between 0 and -50 cmH_2O compared to native trachea, even after only 1 decellularization cycle. Yet, no statistical analysis of these findings was reported. We added a liquid column to control for minor pressure changes and we increased sample-size to detect significance.

Firstly, we established a relevant pressure-range for biomechanical testing. Within this tested range, rabbit tracheae that had undergone eight cycles of detergent-enzymatic decellularization displayed significantly increased collapsibility or malacia compared to native tracheae, especially within the higher pressure-ranges. Collapse was primarily caused by bulging of the trachealis muscle into the lumen at mild negative pressure-differences, whilst additional bowing of the cartilage occurred mainly at higher negative pressure-differences. Nevertheless, unlike other groups [8,9,15,16], we were unable to determine a significant decrease of total collagen or sGAGs in our samples. Also histological analysis did not demonstrate marked collagen-fiber disorganization within the cartilage of eight-cycle constructs. These results indicate that the

employed microCT-technique revealed biomechanical instabilities, which would otherwise have remained undetected by our quantitative and qualitative analyses.

An important advantage of this technique is its non-disruptive character. In contrast with uniaxial mechanical testing, during which tracheae are subjected to increased traction up until rupture of the scaffold, this scanning method enabled us to measure tracheal collapsibility up to -100 cmH_2O without causing permanent structural deformation. Within the positive pressure range, rabbit tracheae tended to become stretched out after applying pressure above 80 cmH_2O. As tracheal detergent-enzymatic decellularization mainly affected collapsibility in our series, this method might be used as a safety-step prior to clinical implementation of natural or synthetic tubular scaffolds. We established this relevant pressure-range, i.e. between -100 cmH_2O and +80 cmH_2O, in humans. Further studies should be conducted to test the biomechanical behavior of human decellularized trachea and to verify whether the technique is also non-destructive for human trachea within this range. If human trachea shows equal preservation of its structure, we postulate that pre-clinical biomechanical testing of tracheae with microCT between -100 cmH_2O and +80 cmH_2O might mark a safe threshold for future implantation. Moreover, this technique may be implemented as a tool for testing the mechanical properties of other tubular constructs such as vascular conduits. For each species or tissue, a maximum of decellularization cycles may thus be determined.

The number of decellularization cycles required to remove all non-cartilaginous cells appears to be consistently low in all species, compared to the discordantly high number of cycles needed to achieve near-complete chondrocyte removal. Cartilage immunology has been studied extensively in the field of articular cartilage transplantation [24]. Embedded into their dense, avascular matrix, chondrocytes are assumed to be protected from a distinct immune response [25], though a harmful event directed towards the cartilage could potentially lead to exposure of these cells and trigger an immune response [26]. We witnessed a significant drop in DNA-content of the decellularized rabbit construct after 2 to 8 cycles compared to native tissue, though a mean DNA-content of 105 ng/mg was still present in the scaffolds after 8 cycles. Histological analysis showed that cells outside the cartilage were removed within 2 cycles, but that even after 8 cycles, cellular material was still present within the cartilage. According to general criteria of decellularization, no more than 50 ng dsDNA per mg ECM dry weight may remain within the tissue if negative remodeling responses are to be avoided [27]. This threshold concentration has not yet been established specifically for

tracheal tissue. Tracheal tissue exhibits multiple characteristics with various responses to the decellularizing treatment. If the immune-privileged status of the cartilage proves to be correct, a higher cartilaginous DNA-concentration, above the threshold, might be tolerated.

Because of the absence of a well-defined vascular pedicle, effective decellularization of the trachea by means of perfusion is unfeasible. Detergent-enzymatic decellularization is achieved by immersion and mechanical agitation. The ECM must inevitably be disrupted [7] to allow for exposure of cells to the ionic detergent and enzyme and to provide a path for removal of the resulting cellular debris. Disturbance of ECM-organization might thus be attributed to the mechanism of action of these agents [7,28]. One might expect that after a certain exposure dose and/or time, the extent of ECM-disruption will be sufficiently large to cause repercussions, in terms of both mechanical disturbances and impairment of adequate cell migration on *in-vivo* implantation. Indeed, after 8 cycles of decellularization, SEM showed substantial disruption of the supportive *lamina basalis*, which acts as a platform for linear, non-invasive outgrowth of epithelium [29]. Absence of this barrier might hamper effective epithelial-cell seeding drastically. Too little exposure to decellularizing agents on the other hand, will cause insufficient removal of immunogenic material and graft rejection. This includes profound removal of nuclear remnants that eagerly stick onto extracellular elements [8,30]. In addition, proper washout of detergent-enzymatic residua is crucial to control the *in-vivo* host response [31]. To maintain a proper balance, tracheae should clearly receive the most gentle treatment that allows for adequate cell-removal and washout. Our data showed that eight cycles of exposure to detergent and enzyme led to loss of normal mechanical characteristics, even before complete chondrocyte-removal and before significant loss of collagen or sGAGs.

After implantation, substantial weakening of eight-cycle decellularized constructs was seen. These scaffolds showed massive inflammation and absent flap integration. Although we did not quantify the amount of residual detergent or enzyme within the scaffold, we hypothesize this inflammation might be caused by these pro-inflammatory remnants. No immunological response was seen directed towards the cartilage of two- and four-cycle constructs, despite the persistence of allogenic chondrocytes within lacunae. These findings imply that gentle tracheal decellularization could provide sufficient removal of allogenic cells of non-cartilaginous tissue, with preserved biomechanics. In search for the most gentle, effective treatment, the preferred result for rabbit

trachea might be achieved after only two decellularizing cycles. Heterotopic revascularization of autologous tracheae occurs via the posterior trachealis muscle and via the intercartilaginous ligaments [22,32]. In our series, submucosal outgrowth of blood vessels was insufficient in all constructs after three weeks of prelamination. Possibly, this insufficiency was related to interference with submucosal detergent-enzymatic residua. Future experiments should focus on extensive washout of scaffolds, to elucidate whether two-cycle decellularized tracheae indeed show favorable integration after *in-vivo* implantation.

We tested rabbit tracheae within a human pressure-range. Presumably, rabbit tracheae are subjected to smaller pressure-changes and our findings may not be directly translated to humans. The aim of this experiment however, was to evaluate whether this method would gain valuable biomechanical information within a near-physiologic pressure-range rather than obtaining absolute values specifically for rabbits. The rabbit trachealis muscle encompasses only 10% of tracheal circumference, in contrast to 30% in humans. As collapse was primarily caused by bulging of the trachealis muscle into the lumen in our study, decellularized human grafts might be even more prone to collapse. Another remark is the static nature of our set-up. O'Donnell *et al* concluded that the magnitude of static end-expiratory tracheal collapse does not predict excessive dynamic expiratory tracheal collapse in COPD patients [33]. Further research should elucidate whether dynamic measurements would support our results. Moreover, the above-mentioned difference in submucosal presence of glandular components between rabbits and humans [22,23] might explain why we did not observe residual nuclear material within submucosal glands, which has been repeatedly established in porcine trachea [8,17,34]. However, to ascertain this cellular clearance, DNA-content needs to be quantified specifically for non-cartilaginous tissues as well. H&E and DAPI-staining approximated DNA-clearance in our series, but may not be equalized to exact quantification methods such as an agarose gel-electrophoresis to determine the length of remaining DNA-strands [7,8]. Lastly, it is now recognized that scaffold-associated macrophages play a key role in the host response to decellularized matrices. Sadtler *et al* demonstrated that a T-helper 2 response is needed for remodeling of ECM-scaffolds (REF). Future work should identify to which extent these pro-regenerative cells are present in implanted decellularized tracheal scaffolds [35].

To conclude, this study elaborated a novel, innovative concept for testing tracheal biomechanics. Presently, no valid method exists for evaluating non-linear tubular constructs. MicroCT-based

volume rendering of inflated and deflated circumferential scaffolds was an elegant technique to test samples unambiguously over the required length. Practical setup was easily feasible. The technique provides good detail of individual components, e.g. cartilage and muscle, as well as the aggregate behavior of the organ. Moreover, in contrast with traditional, uniaxial testing methods, this technique was non-destructive. As such, it might be implemented as a quality-control step for newly developed constructs. Other criteria such as spectrophotometric quantification and histological analysis do not necessarily detect relevant mechanical disturbances. We first established a physiological range of pressure-differences to which human trachea is subjected. Within this range, we were able to detect important loss of biomechanical functional integrity of rabbit trachea with progressive cycles of decellularization, an unfavorable behavior not observed at lower cycle-numbers. *In-vivo* implantation of 8-cycle constructs also showed substantial weakening. This mechanical instability was not revealed by our quantitative nor qualitative architectural analyses. Therefore, we propose a physiological model might yield important progress in pre-clinical mechanical optimization of tracheae, without permanent deformation of the scaffold. In search for the most gentle, effective treatment with preservation of biomechanical properties, the preferred result for rabbit trachea might be achieved after only two detergent-enzymatic decellularization-cycles.

Funding sources

This work was supported by the predoctoral fellowship of the Research Foundation Flanders, Belgium [FWO; 11I0413N] of MDH. CRB and EFM were funded by the Wellcome Clinical Research Training Program. CC was funded by the GOSH Charity Program.

Disclosures

The authors of this manuscript have no conflicts to disclose as described by *Acta Biomaterialia*.

Figures

Fig. 1. MicroCT was used to measure tracheal collapsibility and expandability. *a.* Full length of suspended tracheae measured 6 cm (blue arrow). The red arrow depicts the length of the trachea between the sealed ends. The scanned tracheal length (green arrow) was centered over the tube to avoid measurement errors close to the fixation points. *b.* Tracheae were mounted onto the pressure system before entering the Skyscan microCT. *c.* Pressure-changes were set from 0 cmH_2O to +80 cmH_2O and -100 cmH_2O at room temperature, with intervals of 20 cmH_2O. Pressure was exerted onto the trachea via the syringe. *d.* Radiography showing a collapsed 8-cycle trachea at -80 cmH_2O.

Fig. 2. Three-dimensional volume rendering of axial microCT-images of native and decellularized trachea demonstrated increased collapsibility of constructs after eight cycles of decellularization by detergent-enzymatic method (DEM). Scale bars for the 3D-images represent 1 mm.

Fig. 3. Tracheal collapsibility and expandability were measured after 2, 4 and 8 cycles of detergent-enzymatic decellularization, and compared to native trachea. For comparison purposes, displayed volumes were expressed as volume at the given pressure-difference (cm^3) divided by resting volume at 0 cmH_2O (cm^3). Each data point represents the mean ± SEM of six independently measured tracheae.

Fig. 4. *a.* Total DNA significantly decreased between native tracheae and 2-8 cycle-tracheae, between cycle 1 and cycle 3-8, between cycle 2 and cycle 4-8 and between cycle 3 and cycle 6, after which no further significant drops with successive decellularization cycles were observed. We found no significant decrease in sGAG (*b*) or collagen (*c*) of whole trachea up to 8 decellularization cycles. Total collagen increased significantly after 8 cycles compared to native tracheae and 2-cycle tracheae.

Fig. 5. H&E, Masson Trichrome and DAPI staining showed the presence of nuclear material within the cartilage up to 8 cycles of detergent-enzymatic decellularization. On PAS staining, thinning and local disruption of the basement membrane after 8 cycles of decellularization was visible. Picrosirius red stain, visualized under polarizing light, did not detect an alteration of collagen organization within the outer cartilaginous layers. The framework of the submucosal capillary plexus was preserved up to 8 cycles. However, the stain suggested less-organized collagen fibers near the basement membrane of 8-cycle tracheae. Safranin O staining confirmed the preservation of GAGs within the cartilage up to 8 cycles. Von Kossa staining showed a similar extracellular calcification pattern within the cartilage of native trachea, compared to tracheae after 2, 4 and 8 cycles of decellularization.

Fig. 6. Scanning electron microscopy (SEM) of tracheae showing luminal surface. *a.* Pseudostratified ciliated epithelium of native trachea; x1500. Successful removal of epithelium with intact fibronectin, i.e. *lamina densa* of basement membrane, after 2 cycles (*b*; x 200) and 4 cycles of DEM (*c*; x1000). *d.* Partial destruction of basement membrane with exposure of underlying reticular collagen fibrils after 8 cycles of DEM; x500. *e.* 8-cycle DEM x2500.

Fig. 7. SEM of tracheae focusing on the cartilaginous surface. *a.* Native trachea; x200. Trachea after 2 cycles (*b*; x 200) and 4 cycles of DEM showed a preservation of the cartilaginous architecture (*c*; x50). *d.* Nuclear material within the cartilage remained present up to 8 cycles of decellularization. The extracellular matrix of this group appeared less hydrated; x200.

Fig. 8. 2-cycle decellularized trachea wrapped within the lateral thoracic artery flap [22] showed excellent luminal patency on postoperative (POD) 0 (*a*) and POD 14 (*b*). Incomplete submucosal revascularization was visible on H&E-stain after three weeks of heterotopic prelamination (*c*). Scarce CD4/8+ lymphocytes were present within the adventitia (*d*, arrows). *e.* Implanted 8-cycle tracheae on POD 14 showed extensive inflammation internally and externally. Flap-ingrowth was unsuccessful. *f.* Collapse of 8-cycle construct on POD 21. Neutrophilic infiltration was confirmed on

H&E stain (*g, curly brackets*), with only few CD4/8+ lymphocytes at the implant-host interface (*h*, arrows).

Table

Pressure-difference	P-value native vs. cycle 2	P-value native vs. cycle 4	P-value native vs. cycle 8	P-value cycle 2 vs. cycle 4	P-value cycle 2 vs. cycle 8	P-value cycle 4 vs. cycle 8
+80 cmH_2O	1	1	1	1	1	1
+60 cmH_2O	1	1	0.671	1	1	1
+40 cmH_2O	1	1	0.282	1	1	1
+20 cmH_2O	1	1	1	1	1	1
0 cmH_2O	1	1	1	1	1	1
-20 cmH_2O	0.313	0.085	0.085	1	1	1
-40 cmH_2O	1	0.436	**0.012**	1	0.481	1
-60 cmH_2O	1	0.222	**0.002**	1	0.074	0.744
-80 cmH_2O	0.572	0.124	**0.002**	1	0.267	1
-100 cmH_2O	1	0.165	**0.002**	0.948	**0.024**	0.811

Table 1. Statistical analysis using the 2-way ANOVA-test with Bonferroni post-testing found significantly increased collapsibility of 8-cycle tracheae ≤ -40 cmH_2O. Each group comprised six tracheae (n_{total} = 24). P-values below 0.05 were considered statistically significant.

References

[1] N.J. Hamilton, M. Kanani, D.J. Roebuck, R.J. Hewitt, R. Cetto, E.J. Culme-Seymour, E. Toll, A.J. Bates, A.P. Comerford, C.A. McLaren, C.R. Butler, C. Crowley, D. McIntyre, N.J. Sebire, S.M. Janes, C. O'Callaghan, C. Mason, P. De Coppi, M.W. Lowdell, M.J. Elliott, M.A. Birchall,Tissue Engineered Tracheal Replacement in a Child: A 4-Year Follow-Up Study, Am. J. Transplant. 15 (2015) 2750-2757.

[2] A. Gonfiotti, M.O. Jaus, D. Barale, S. Baiguera, C. Comin, F. Lavorini, G. Fontana, O. Sibila, G. Rombolà, P. Jungebluth, P. Macchiarini, The first tissue-engineered airway transplantation: 5-year follow-up results, Lancet. 383 (2014) 238-244.

[3] P. Jungebluth, E. Alici, S. Baiguera, K. Le Blanc, P. Blomberg, B. Bozóky, C. Crowley, O. Einarsson, T. Gudbjartsson, S. Le Guyader, G. Henriksson, O. Hermanson, J.E. Juto, B. Leidner, T. Lilja, J. Liska, T. Luedde, V. Lundin, G. Moll, C. Roderburg, S. Strömblad, T. Sutlu, E. Watz, A. Seifalian, P. Macchiarini, Tracheobronchial transplantation with a stem-cell-seeded bioartificial nanocomposite: a proof-of-concept study, Lancet. 378 (2011) 1997-2004.

[4] D. Weiss, M. Elliott, Q. Jang, B. Poole, M. Birchall, International Society of Cell Therapy Pulmonary Scientific Committee, Tracheal bioengineering: the next steps. Proceeds of an International Society of Cell Therapy Pulmonary Cellular Therapy Signature Series Workshop, Paris, France, April 22, 2014, Cytotherapy. 16 (2014) 1601–1613.

[5] P. Delaere, J. Vranckx, G. Verleden, P. De Leyn, D. Van Raemdonck, Leuven Tracheal Transplant Group, Tracheal Allotransplantation after Withdrawal of Immunosuppressive Therapy, New Engl. J. Medicine. 362 (2010) 138–145.

[6] P. Delaere, J. Vranckx, J. Meulemans, V. Vander Poorten, K. Segers, D. Van Raemdonck, P. De Leyn, H. Decaluwé, C. Dooms, G. Verleden, Learning Curve in Tracheal Allotransplantation,

Am. J. Transplant. 12 (2012) 2538–2545.

[7] T.W. Gilbert, T.L. Sellaro, S.F. Badylak, Decellularization of tissues and organs, Biomaterials. 27 (2006) 3675-3683.

[8] L. Partington, N. J. Mordan, C. Mason, J.C. Knowles, H.W. Kim, M.W. Lowdell, M.A. Birchall, I.B. Wall, Biochemical changes caused by decellularization may compromise mechanical integrity of tracheal scaffolds, Acta Biomater. 9 (2013) 5251-5261.

[9] M. Zang, Q. Zhang, E.I. Chang, A.B. Mathur, P. Yu, Decellularized tracheal matrix scaffold for tissue engineering, Plast. Reconstr. Surg. 130 (2012) 532-540.

[10] P. Jungebluth, T. Go, A. Asnaghi, S. Bellini, J. Martorell, C. Calore, L. Urbani, H. Ostertag, S. Mantero, M.T. Conconi, P. Macchiarini, Structural and morphologic evaluation of a novel detergent-enzymatic tissue-engineered tracheal tubular matrix, J. Thorac. Cardiovasc. Surg. 138 (2009) 586-593.

[11] S. Baiguera, P. Jungebluth, A. Burns, C. Mavilia, J. Haag, P. De Coppi, P. Macchiarini, Tissue engineered human tracheas for in vivo implantation, Biomaterials. 31 (2010) 8931-8938.

[12] C.R. Roberts, J.K. Rains, P.D. Paré, D.C. Walker, B. Wiggs, J.L. Bert, Ultrastructure and tensile properties of human tracheal cartilage, J. Biomech. 31 (1998) 81-86.

[13] O. Trabelsi, A.P. del Palomar, J.L. López-Villalobos, A. Ginel, M. Doblaré, Experimental characterization and constitutive modeling of the mechanical behavior of the human trachea, Med. Eng. Phys. 32 (2010) 76-82.

[14] Z. Teng, I. Ochoa, Z. Li, M. Doblaré, Study of tracheal collapsibility, compliance and stress by considering its asymmetric geometry, Med. Eng. Phys. 31 (2009) 328-336.

[15] F. Sun, S. Pan, H. Shi, F. Zhang, W. Zhang, G. Ye, X.C. Liu, S.Q. Zhang, C.H. Zhong, X.L. Yuan, Structural integrity, immunogenicity and biomechanical evaluation of rabbit decellularized tracheal matrix, J. Biomed. Mater. Res. A. 103 (2015) 1509–1519.

[16] S. Haykal, J.P. Soleas, M. Salna, S.O. Hofer, T.K. Waddell, Evaluation of the structural integrity and extracellular matrix components of tracheal allografts following cyclical decellularization techniques: comparison of three protocols, Tissue Eng. Part C Methods. 18 (2012) 614-623.

[17] M.T. Conconi, P. De Coppi, R. Di Liddo, S. Vigolo, G.F. Zanon, P.P. Parnigotto, G.G. Nussdorfer, Tracheal matrices, obtained by a detergent-enzymatic method, support in vitro the adhesion of chondrocytes and tracheal epithelial cells, Transpl. Int. 18 (2005) 727-734.

[18] E. Meezan, J.T. Hjelle, K. Brendel, E.C. Carlson, A simple, versatile, nondisruptive method for the isolation of morphologically and chemically pure basement membranes from several tissues, Life Sci. 17 (1975) 1721-1732.

[19] P. Macchiarini, P. Jungebluth, T. Go, M.A. Asnaghi, L.E. Rees, T.A. Cogan, A. Dodson, J. Martorell, S. Bellini, P.P. Parnigotto, S.C. Dickinson, A.P. Hollander, S. Mantero, M.T. Conconi, M.A. Birchall, Clinical transplantation of a tissue-engineered airway, Lancet. 372 (2008) 2023-2030.

[20] M.J. Elliott, P. De Coppi, S. Speggiorin, D. Roebuck, C.R. Butler, E. Samuel, C. Crowley, C. McLaren, A. Fierens, D. Vondrys, L. Cochrane, C. Jephson, S. Janes, N.J. Beaumont, T. Cogan, A. Bader, A.M. Seifalian, J.J. Hsuan, M.W. Lowdell, M.A. Birchall, Stem-cell-based, tissue engineered tracheal replacement in a child: a 2-year follow-up study, Lancet. 380 (2012) 994-1000.

[21] G. Totonelli, P. Maghsoudlou, M. Garriboli, J. Riegler, G. Orlando, A.J. Burns, N.J. Sebire, V.V. Smith, J.M. Fishman, M. Ghionzoli, M. Turmaine, M.A. Birchall, A. Atala, S. Soker, M.F. Lythgoe, A. Seifalian, A. Pierro, S. Eaton, P. De Coppi, A rat decellularized small bowel scaffold that preserves villus-crypt architecture for intestinal regeneration, Biomaterials. 33 (2012) 3401-3410.

[22] M. Den Hondt, B. Vanaudenaerde, P. Delaere, J.J. Vranckx, Twenty years of experience with the rabbit model, a versatile model for tracheal transplantation research, Plast. Aesthet. Res. 3 (2016) 223-230.

[23] J.R. Salassa, B.W. Pearson, W.S. Payne, Gross and microscopical blood supply of the trachea, Ann. Thorac. Surg. 24 (1977) 100-107.

[24] L. Bolano, J.A. Kopta, The immunology of bone and cartilage transplantation, Orthopedics. 14 (1991) 987-996.

[25] M. Sykes, Immune Evasion by Chimeric Trachea, N. Engl. J. Med. 362 (2010) 172–174.

[26] S. Heyner, The significance of the intercellular matrix in the survival of cartilage allografts, Transplantation. 8 (1969) 666-677.

[27] P.M. Crapo, T.W. Gilbert, S.F. Badylak, An overview of tissue and whole organ decellularization processes, Biomaterials. 32 (2011) 3233-3243.

[28] A.M. Seddon, P. Curnow, P.J. Booth, Membrane proteins, lipids and detergents: not just a soap opera, Biochim. Biophys. Acta. 1666 (2004) 105-117.

[29] V.S. LeBleu, B. MacDonald, R. Kalluri, Structure and Function of Basement Membranes, Exp. Biol. Med. 232 (2007) 1121-1129.

[30] T.J. Keane, R. Londono, N.J. Turner, S.F. Badylak, Consequences of ineffective decellularization of biologic scaffolds on the host response, Biomaterials. 33 (2012) 1771-1781.

[31] S. Cebotari, I. Tudorache, T. Jaekel, A. Hilfiker, S. Dorfman, W. Ternes, A. Haverich, A. Lichtenberg, Detergent decellularization of heart valves for tissue engineering: toxicological effects of residual detergents on human endothelial cells, Artif. Organs. 34 (2010) 206-210.

[32] P.R. Delaere, Z. Liu, P. Pauwels, L. Feenstra, Experimental revascularization of airway segments, Laryngoscope. 104 (1994) 736-740.

[33] C.R. O'Donnell, A.A. Bankier, D.H. O'Donnell, S.H. Loring, P.M. Boiselle, Static end-expiratory and dynamic forced expiratory tracheal collapse in COPD, Clin Radiol. 69 (2014) 357-362.

[34] S. Haykal, Y. Zhou, P. Marcus, M. Salna, T. Machuca, S.O. Hofer, T.K. Waddell, The effect of decellularization of tracheal allografts on leukocyte infiltration and of recellularization on regulatory T cell recruitment, Biomaterials. 34 (2013) 5821-5832.

[35] Developing a pro-regenerative biomaterial scaffold microenvironment requires T helper 2 cells, Science. 352 (2016) 366-370.